ARL-TN-1007 • FEB 2020

High-Speed Video of Electric Arcs and Exploding Wires

by Brian L Wilmer, Matthew J Coppinger, and Willard C Uhlig

NOTICES

Disclaimers

The findings in this report are not to be construed as an official Department of the Army position unless so designated by other authorized documents.

Citation of manufacturer's or trade names does not constitute an official endorsement or approval of the use thereof.

Destroy this report when it is no longer needed. Do not return it to the originator.

ARL-TN-1007 ● FEB 2020

High-Speed Video of Electric Arcs and Exploding Wires

Brian L Wilmer
SURVICE Engineering Company

Matthew J Coppinger and Willard C Uhlig
Weapons and Materials Research Directorate, CCDC Army Research Laboratory

REPORT DOCUMENTATION PAGE

Form Approved
OMB No. 0704-0188

1. REPORT DATE *(DD-MM-YYYY)*	2. REPORT TYPE	3. DATES COVERED (From - To)
February 2020	Technical Note	11/1/2019–1/1/2020

4. TITLE AND SUBTITLE
High-Speed Video of Electric Arcs and Exploding Wires

5a. CONTRACT NUMBER

5b. GRANT NUMBER

5c. PROGRAM ELEMENT NUMBER

6. AUTHOR(S)
Brian L Wilmer, Matthew J Coppinger, and Willard C Uhlig

5d. PROJECT NUMBER

5e. TASK NUMBER

5f. WORK UNIT NUMBER

7. PERFORMING ORGANIZATION NAME(S) AND ADDRESS(ES)
CCDC Army Research Laboratory
ATTN: FCDD-RLW-PA
Aberdeen Proving Ground, MD 21005

8. PERFORMING ORGANIZATION REPORT NUMBER
ARL-TN-1007

9. SPONSORING/MONITORING AGENCY NAME(S) AND ADDRESS(ES)

10. SPONSOR/MONITOR'S ACRONYM(S)

11. SPONSOR/MONITOR'S REPORT NUMBER(S)

12. DISTRIBUTION/AVAILABILITY STATEMENT
Approved for public release; distribution is unlimited.

13. SUPPLEMENTARY NOTES
ORCID ID(s): Willard C Uhlig, 0000-0003-1815-0106

14. ABSTRACT
High-speed photography of high-voltage spark gaps and exploding wires is presented. Various filters, camera, and laser configurations are tested to explore what data may be acquired.

15. SUBJECT TERMS
shadowgraphy, exploding wires, spark gaps, laser illumination, pulsed power

16. SECURITY CLASSIFICATION OF:			17. LIMITATION OF ABSTRACT	18. NUMBER OF PAGES	19a. NAME OF RESPONSIBLE PERSON
a. REPORT	b. ABSTRACT	c. THIS PAGE			Brian L Wilmer
Unclassified	Unclassified	Unclassified	UU	17	19b. TELEPHONE NUMBER (Include area code) (410) 278-7315

Contents

Acknowledgments

The authors would like to thank Colby Adams and Robert Borys for their technical assistance conducting the experiments.

List of Figures

List of Tables

1. Introduction

High current electrical discharges generate bright, broadband emission from both the electric arc itself and resultant hot plasma. X-rays are able to penetrate this interference; however, information is limited to dense material and a small number of images. Therefore, a Shimadzu HPV X2 camera, which is capable of up to 10 Mfps and 50-ns exposures with combinations of various filters and a CAVILUX Smart Laser Unit illuminator, was employed to explore optical imaging possibilities. Two imaging scenarios are considered in this work. First, the capabilities of the camera are evaluated by imaging an electric arc formed between two electrodes both when directly viewing the arc and using shadowgraphy. Second, an exploding wire is imaged under laser illumination.

2. Optical Filters

To match the wavelength of the near-infrared (NIR) Cavilux illuminator, an 810-nm bandpass filter was used on the camera. An ultraviolet (UV) filter was in place for all measurements, which reduced transmission by 15% across the whole spectrum. While UV protection is not necessary due to the 810-nm bandpass, this filter is a practical measure to protect the camera lens from any mechanical damage from debris. In addition to the spectral filter, further attenuation is achieved with neutral density (ND) filters and f-stops. ND filters are spectrally flat attenuators and their performance is defined by their optical density:

$$Optical\ Density\ (OD) = -log_{10}\left(\frac{I_t}{I_i}\right),$$

where I_t and I_i are the transmitted and incident intensities, respectively. An "ND 3" filter attenuates incident light by 1000, for example. F-stops are achieved by mechanically blocking light entering the detector via a built-in adjustable aperture. F-stop is defined as the ratio of the lens focal length to aperture diameter:

$$f - stop = \frac{f_{lens}}{d_{aperature}}.$$

Very generally, larger f-stops preferentially allow more collimated light to pass through the system, increasing the depth of view at the cost of decreasing the overall amount of light (less collimated) entering the sensor. To convert between f-stop and OD, the conversion factor 1 f-stop = 0.3 OD can be used. In this work, ND filters were chiefly employed for attenuation and low f-stops for a shallow depth of view.

A 0.25-inch-diameter solid copper rod was used to make a 0.02-inch spark gap, which nominally broke down at 2.5 kV. Table 1 shows a summary of the observed intensity as a function of attenuation. The sampling rate (i.e., frame rate) was fixed at 1 Mfps and the exposure was fixed at 200 ns. The Shimadzu recording length is 256 frames, thus 256 μs at a 1-Mfps frame rate.

Table 1 Summary data for viewing spark gaps with different attenuation

Shot	f-stop	Filters	Max % of dynamic range	Number of frames with max %	Over saturated pixels?
1	5.6	UV, ND 2.1	100	255	Yes
2	5.6	UV, NIR, ND 2.1	100	250	Yes
3	2.8	UV, NIR, ND 3	100	114	No
4	2.8	UV, NIR, ND 3.9	100	1	No
5	2.8	UV, NIR, ND 4.8	7	1	No

The relative intensity measurement, quantified as the maximum percentage of the camera's dynamic range, is derived from the three pixels of highest intensity in each frame of each shot. Each frame was passed through a median filter in MatLab, which replaces the value in each pixel with the median value of a 3 × 3 pixel grid centered on each pixel. In all cases, the three highest-intensity (not necessarily saturated) pixels in each individual frame were equal. The duration of maximum intensity is quantified as the number of frames with three or more pixels at the shot's maximum. In the case of light intensity far exceeding the sensor's dynamic range, the Shimadzu's pixels register 0 counts. Therefore, very bright light appears black in the central, brightest regions. As a result, no quantitative intensity analysis is possible in these regions. Representative frames with peak intensities from these videos are shown in Fig. 1. In all spark gap recordings, oscillations in the radiant intensity of the air plasma as a result of the RLC circuit were visible.

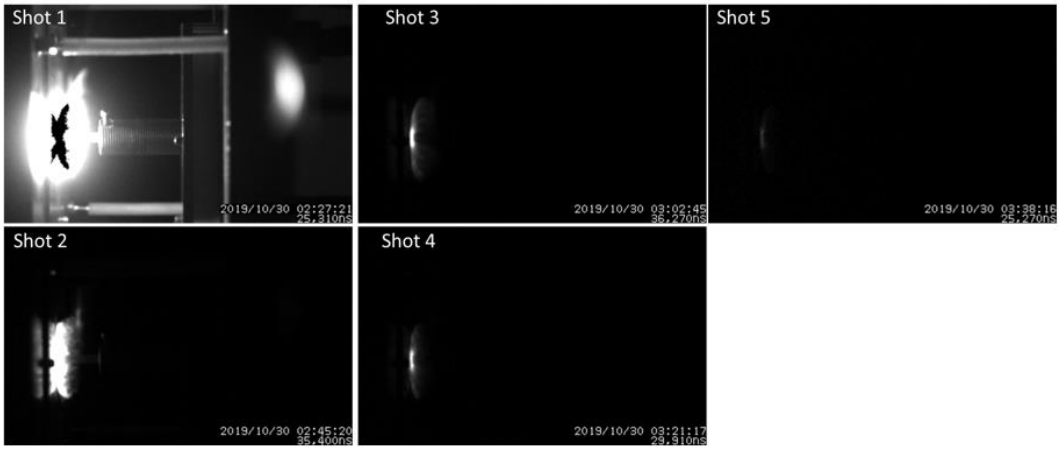

Fig. 1 Individual frames from the videos of shots in Table 1. The frames show the maximum intensity observed during each shot. Shot 5's brightness was enhanced 50% for visibility.

3. Shadowgraphy

By backlighting an object and imaging the resulting shadow to generate shadowgraphs, one can track an object more easily at high speed as less light is necessary compared to reflection photography. The CAVILUX Smart Laser Unit illuminator generates 400-W, 806-nm pulses. The pulses are divergent, spatially homogenous, and temporally variable in increments of 10 ns from 10 ns–200 µs. The pulses are in phase with exposure via a synchronization signal from the Shimadzu camera. In this work, the laser's light was collimated with a 4-inch-diameter, 8-inch focal length lens to a spot size of approximately 1.5-inch in diameter. Table 2 shows a summary of the recording parameters used for imaging the spark gap. There were no overly saturated pixels at these attenuations.

Table 2 Summary data for viewing spark gaps with laser illumination backlighting

Shot	f-stop	Filters	Frame rate	Exposure (ns)	Laser pulse width (ns)	Max % of dynamic range	Number of frames at max %
6	2.8	UV, NIR, ND 3.6	1M	200	200	100	150
7	2.8	UV, NIR, ND 4.8	1M	200	200	59	1
8	2.8	UV, NIR, ND 3.6	1M	250	10	100	2
9	4	UV, NIR, ND 3.6	10M	50	50	100	181

Shot 6 remains saturated in the region illuminated by the CAVILUX throughout the exposures with an ND 2.6 (Fig. 2). In shot 7 (ND 4.8), multiple shock waves emanating from the spark gap are visible with little to no light from the arc or plasma (Fig. 3).

Fig. 2 Individual frame from shot 6, spark gap position indicated by red arrow

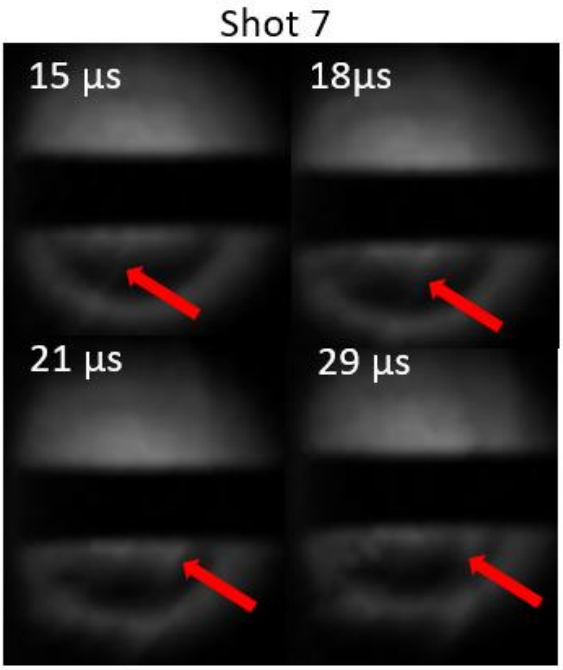

Fig. 3 Frames from shot 7 showing faintly visible shock wave propagation (red arrows)

Shot 8 used a shorter illuminator pulse width of 4% of the exposure period and yields similar data to shot 7 (Fig. 4).

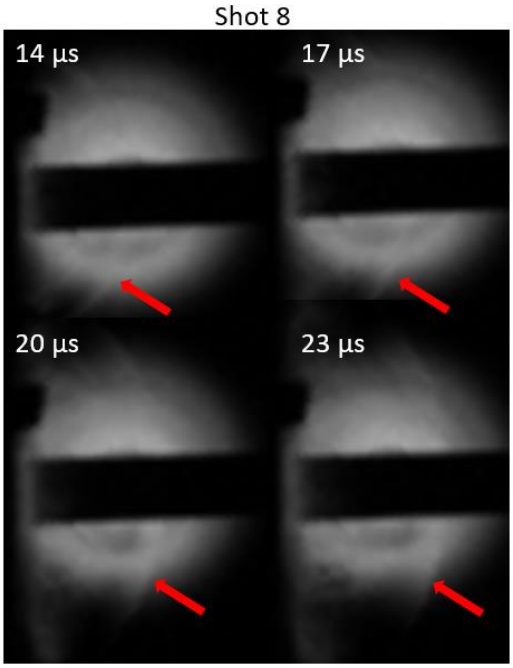

Fig. 4 Frames from shot 8, showing clearer shock wave propagation (red arrows)

In this shot, one can also see material flowing from the copper electrode, indicated by the red arrow in Fig. 5.

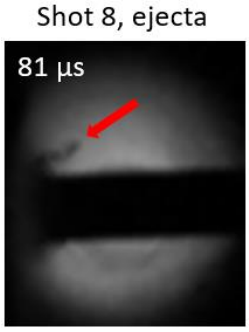

Fig. 5 Frame from shot 8 showing ejected material (red arrow) from the spark gap

While material flow is not observed in shot 7, this behavior is stochastic, and simply may not have occurred during shot 7. Shot 9, with a higher sampling rate of 10 Mfps, shows a single shock wave emanating from the spark gap (Fig. 6).

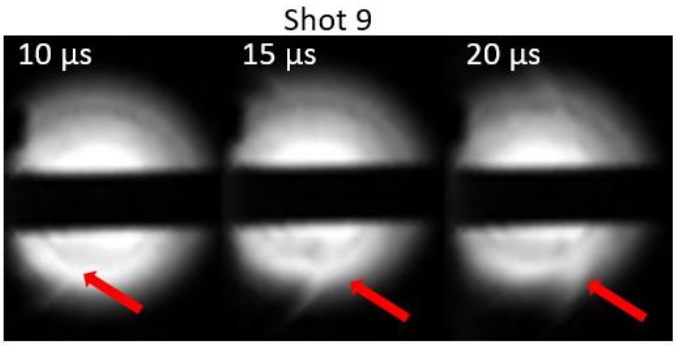

Fig. 6 Frames from shot 9 showing clear propagation of a single shock wave (red arrows)

4. Exploding Wire

An approximately 3.5-inch-long × 0.0625-inch-diameter copper wire was exploded using a 6-kV, 200-kA peak current electrical pulse. These data are summarized in Table 3. In an attempt to "see through" the hot plasma and debris to see the wire exploding, the illuminator's duty cycle was varied in shots 10 and 11 from 5% to 100% (10 to 200 ns) of the exposure, respectively. For this scheme to work, the laser needs to be sufficiently intense to both be brighter than any plasma emission and overcome any losses due to absorption and scatter.

Table 3 Summary data for backlit exploding wire experiments

Shot	f-stop	Filters	Frame rate (Mfps)	Exposure (ns)	Laser pulse width (ns)	Max % of dynamic range	Number of frames at max %
10	2.8	UV, NIR, ND 3.6	1	200	10	100	1
11	2.8	UV, NIR, ND 3.6	1	200	200	100	31

All attempts to see through the plasma and debris with the laser illuminator failed due to strong absorption and scatter from the copper as it vaporized.

In the early stages of explosion, however, one can observe the cross section of the wire expanding, starting at the ends and working toward the center. As the wire begins to vaporize, striations and smoke rings are discernable (Figs. 7 and 8).

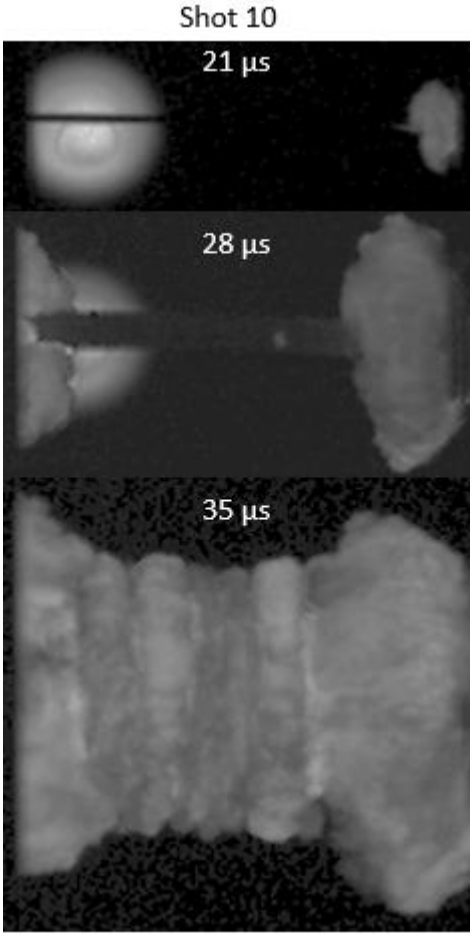

Fig. 7 Frames from shot 10 with the laser illumination at 5% of the exposure, wire cross section expansion and smoke rings in copper vapor are visible

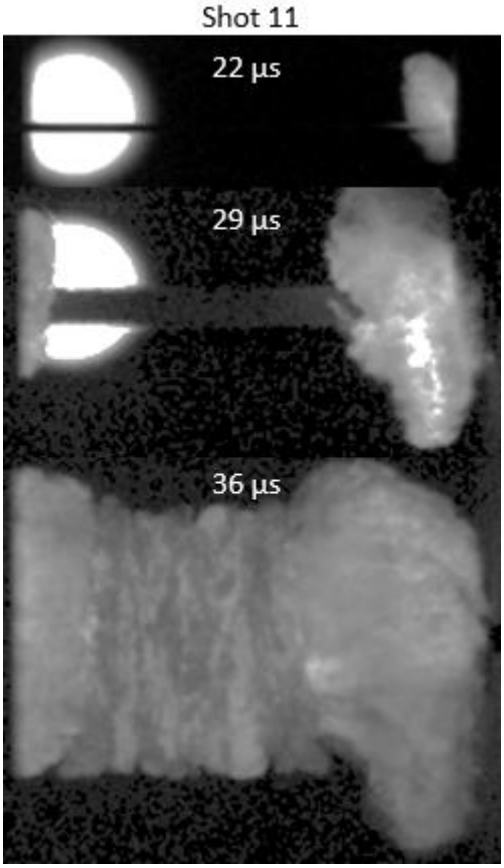

Fig. 8 Frames from shot 11 with the laser illumination at 100% of the exposure, wire cross section expansion and smoke rings in copper vapor are visible

5. Conclusion

In summary, use of a high-speed camera coupled with laser illumination does yield useful quantitative and qualitative information in some typical pulsed power experiments. In spark gaps, the plasma and oscillatory properties of the arc can be observed. With backlighting and attenuation, emission from the air plasma can be overcome and shock waves emanating from the gap are plainly visible. In exploding wire experiments, while it is not possible to see through the exploding wire, one can observe the propagation and smoke rings of the explosion. With backlighting, one can monitor the wire cross section expansion to some extent.

List of Symbols, Abbreviations, and Acronyms

ND	neutral density
NIR	near-infrared
OD	optical density
UV	ultraviolet

1 (PDF)	DEFENSE TECHNICAL INFORMATION CTR DTIC OCA
1 (PDF)	CCDC ARL FCDD RLD CL TECH LIB
3 (PDF)	CCDC ARL FCDD RLW PA B WILMER M COPPINGER W UHLIG